THE ASTROPHYSICAL JOURNAL, 497:L113–L116, 1998 April 20

CALIBRATION OF THE SERTS-95 SPECTROGRAPH FROM IRON LINE INTENSITY RATIOS

JEFFREY W. BROSIUS,[1] JOSEPH M. DAVILA, AND ROGER J. THOMAS
Code 682, NASA Goddard Space Flight Center, Greenbelt, MD 20771
Received 1998 January 6; accepted 1998 February 18; published 1998 March 20

ABSTRACT

Goddard Space Flight Center's Solar EUV Rocket Telescope and Spectrograph was flown on 1995 May 15 (SERTS-95), carrying a multilayer-coated toroidal diffraction grating which enhanced the instrumental sensitivity within its second-order wave band (170–225 Å). Spectra and spectroheliograms of NOAA Active Region 7870 (N09/W22) were obtained in this wave band with a spectral resolution (instrumental FWHM) ~30 mÅ. We developed and applied a technique for deriving the relative radiometric calibration *independent* of laboratory calibration measurements by employing a method proposed by Neupert & Kastner for monitoring variations in the sensitivities of orbiting EUV spectrometers by means of density- and temperature-insensitive line intensity ratios. Numerous ratios of emission lines from Fe X–XIV are mutually consistent and yield an instrumental response curve that matches the design characteristics of the multilayer coating. This supports the accuracy of the atomic physics parameters and demonstrates the power of the technique. Many of the ratios employed here can be used to carry out a similar calibration exercise on spectra from the Coronal Diagnostic Spectrometer's Grazing Incidence Spectrograph (CDS/GIS) aboard the *Solar and Heliospheric Observatory*. Because they are relatively free from blending with nearby strong lines, the following density-sensitive ratios are particularly well suited for analysis with the GIS: Fe X λ175.265/λ174.526, Fe X λ175.265/λ184.534, Fe XII λ186.867/λ195.117, Fe XIII λ203.820/λ202.042, Fe XIII λ200.017/λ202.042, and Fe XIV λ219.121/λ211.317. Densities derived from Fe X, XIII, and XIV yield log $n_e \sim 9.4 \pm 0.2$.

Subject headings: instrumentation: spectrographs — Sun: activity — Sun: corona — Sun: UV radiation

1. INTRODUCTION

Reliable measurements of the density, filling factor, emission measure, and magnetic field strength are essential for understanding the multithermal structures found in the solar corona and for determining the physical processes that occur in those structures. The extreme-ultraviolet (EUV) wave band (150–1200 Å) contains emission lines formed at temperatures ranging from several 10^4 to several 10^7 K and is therefore well suited for studies of those multithermal coronal structures. This is why the EUV wave band was chosen for Goddard Space Flight Center's Solar EUV Rocket Telescope and Spectrograph (SERTS), as well as for the Coronal Diagnostic Spectrometer (CDS) aboard the NASA/ESA *Solar and Heliospheric Observatory* (*SOHO*) spacecraft.

Behring et al. (1976) obtained solar EUV spectra with 60 mÅ spectral resolution during two sounding rocket flights and provided many line identifications. However, those spectra were acquired from full-Sun observations and so provide no information about distinct solar features. Furthermore, the relative line intensities were only approximately calibrated, rendering line intensity ratio measurements uncertain. Observations obtained with the Naval Research Laboratory (NRL) slitless spectrograph on *Skylab* (Tousey et al. 1977) provided high spatial (2″) and spectral (~100 mÅ) resolution images in the 171–630 Å wave band but were limited by the overlap of images from nearby spectral lines. They provided excellent diagnostic capabilities for small, intense sources like flares (e.g., Dere 1978; Dere et al. 1979) but were less well suited for quiet-Sun areas and quiescent active regions.

SERTS (Neupert et al. 1992) was designed to improve on earlier solar EUV instrumentation by (i) retaining the stigmatic imaging capability of the NRL spectroheliograph on *Skylab*, while providing a spatial selection capability that reduces image overlap, and (ii) achieving high spectral resolution (~55/*N* mÅ, where *N* is the spectral order). The configuration of the SERTS entrance aperture enables both spectra and spectroheliograms to be obtained simultaneously: spectra are obtained along a narrow 5′ long slit connecting two rectangular lobes within which the spectroheliograms are imaged. The spatial resolution is ~5″. We discuss only the slit spectra in this work.

The version of SERTS flown in 1989 (SERTS-89) (Neupert et al. 1992; Thomas & Neupert 1994; Young, Landi, & Thomas 1998) carried a standard gold-coated toroidal diffraction grating. It observed hundreds of first-order emission lines between 235 and 450 Å and ~25 second-order lines between 170 and 225 Å. The version of SERTS flown in 1991 (SERTS-91) (Davila et al. 1993; Brosius et al. 1993, 1996a, 1996b) and 1993 (SERTS-93) (Brosius et al. 1996a, 1996b, 1997a, 1997b) carried a multilayer-coated grating that enhanced the instrumental efficiency in the first-order wavelength range, while the version flown in 1995 (SERTS-95) incorporated a multilayer grating that enhanced the sensitivity in the second-order wave band (~170–225 Å). This enhancement brings out many lines that were not seen during any of the previous flights and represents the highest spectral resolution ever achieved for spatially resolved active region and quiet-Sun spectra in this wavelength range (~30 mÅ). The SERTS data and analysis procedure described here should be helpful for ongoing CDS calibration efforts (e.g., Landi et al. 1998a, 1998b).

2. OBSERVATIONS

SERTS was launched on a Terrier-boosted Black Brant rocket from White Sands, New Mexico, at 1800 UT on 1995 May 15. It reached a maximum altitude of 307 km and recorded spectrographic data on photographic film for nearly 7 minutes. The instrument performed well, obtaining four different exposures in each of two different pointing positions. This en-

[1] Raytheon STX Corporation, 4400 Forbes Boulevard, Lanham, MD 20706.

TABLE 1

SERTS-95 Second-Order Calibration Verification from Iron Line Ratios

Ion (1)	Wavelength (λ) (2)	Normalized Theoretical Intensity (3)	Observed Intensity (4)	Normalized Observed Intensity (5)	Col. (5)/Col. (3) (6)
Fe x	174.526	1.000	2.05 ± 0.26	1.00 ± 0.13	1.00 ± 0.13
	177.240	0.619 ± 0.014	1.05 ± 0.15	0.512 ± 0.098	0.827 ± 0.159
	184.534BR	0.256 ± 0.010	0.513 ± 0.075	0.250 ± 0.048	0.977 ± 0.191
	190.046BR	0.078 ± 0.003	0.150 ± 0.029	0.073 ± 0.017	0.943 ± 0.222
Fe xi	181.125	0.402 ± 0.018	0.386 ± 0.111	0.521 ± 0.167	1.30 ± 0.42
	182.166	1.000	0.741 ± 0.104	1.00 ± 0.14	1.00 ± 0.14
Fe xi	188.214BR[a]	1.000	1.21 ± 0.24	1.00 ± 0.20	1.00 ± 0.20
	192.821BR[b]	0.209	0.292 ± 0.054	0.241 ± 0.065	1.15 ± 0.31
Fe xii	186.867[c]	3.58 ± 0.44	1.56 ± 0.20	4.14 ± 0.81	1.16 ± 0.27
	196.642[d]	1.000	0.377 ± 0.056	1.00 ± 0.15	1.00 ± 0.15
Fe xii	192.390	0.212 ± 0.002	0.646 ± 0.079	0.237 ± 0.039	1.12 ± 0.18
	193.505	0.554 ± 0.044	1.53 ± 0.17	0.560 ± 0.089	1.01 ± 0.18
	195.117	1.000	2.73 ± 0.31	1.00 ± 0.11	1.00 ± 0.11
Fe xiii	200.017	1.000	0.954 ± 0.115	1.00 ± 0.12	1.00 ± 0.12
	203.164	0.514 ± 0.091	0.484 ± 0.076	0.507 ± 0.100	0.986 ± 0.261
	203.820[e]	5.18 ± 0.21	6.04 ± 0.75	6.33 ± 1.10	1.22 ± 0.22
	204.255BR	0.652 ± 0.069	0.610 ± 0.093	0.639 ± 0.124	0.980 ± 0.217
	209.623[f]	0.752 ± 0.041	0.657 ± 0.104	0.689 ± 0.137	0.916 ± 0.189
	221.813BR	1.18 ± 0.13	0.684 ± 0.102	0.717 ± 0.137	0.608 ± 0.134
Fe xiii	202.042BR	1.000	3.81 ± 0.43	1.00 ± 0.11	1.00 ± 0.11
	209.908BR[g]	0.170	0.705 ± 0.137	0.185 ± 0.042	1.09 ± 0.25
Fe xiii	201.118BR[h]	1.000	1.47 ± 0.19	1.00 ± 0.13	1.00 ± 0.13
	204.950BR[i]	0.293	0.837 ± 0.139	0.569 ± 0.120	1.94 ± 0.41
Fe xiv	211.317BR	1.000	7.87 ± 0.90	1.00 ± 0.11	1.00 ± 0.11
	220.090BR	0.211	1.95 ± 0.26	0.248 ± 0.044	1.18 ± 0.21

Notes.—The "BR" designation indicates lines in a given series that originate from the same upper level; the intensity ratio corresponds to the *branching ratio*. The following lines observed (footnotes a–i) in the SERTS-95 active region spectrum are within ±0.3 Å of the emission lines listed in col. (2); values in parentheses are the relative intensities and associated uncertainties.

[a] Ar xiv λ187.962 (0.0825 ± 0.0269), Fe xi λ188.295 (0.867 ± 0.162), unidentified λ188.494 (0.112 ± 0.026).

[b] Possible blend with O v.

[c] Ca xiv λ186.616 (0.243 ± 0.049).

[d] Fe xiii λ196.519 (0.423 ± 0.105).

[e] Unidentified λ203.727 (1.63 ± 0.22).

[f] Fe xiii λ209.908 (0.705 ± 0.137).

[g] Fe xiii λ209.623 (0.657 ± 0.104).

[h] Ca xv λ200.978 (0.371 ± 0.063).

[i] Fe xvii λ204.665 (0.226 ± 0.077).

sured the availability of optimally exposed spectral lines and spectroheliograms for both strong and weak spectral features and provided the information needed to determine the film's density versus log energy (D–log E) relation (e.g., Thompson et al. 1993). The wavelength scale was determined from laboratory measurements of He ii and Ne ii lines.

Spectroheliograms of NOAA Active Region 7870 (N09/W22) were obtained in the first pointing position, and spectra of this region were obtained in the second. The narrow slit bisected the region at a 24°.4 angle counterclockwise from the solar rotation axis. Data were digitized with a Perkin-Elmer microdensitometer, and plate flaws were subsequently removed by replacing occasional defects with uncontaminated local pixel averages.

Spectra are available for each spatial pixel along the narrow slit; however, for the present work, we averaged together the 3′.76 segment corresponding to region 7870 in order to enhance the signal-to-noise ratio and therefore acquire as many spectral lines as possible for calibration and density analyses. The longest duration exposure (202.2 s) was used to obtain the averaged spectrum in this work. The background level (due to film fog, scattered light, and actual solar continuum) was determined by removing emission-line candidates from the initial spatially averaged spectrum, replacing them with appropriate local averages, and smoothing the remainder. This background was subtracted from the initial spectrum, leaving only an emission-line spectrum. Emission lines in the background-corrected spectrum were fitted with Gaussian profiles to derive the integrated line intensity and the FWHM, as well as the uncertainty associated with each. Values of the integrated line intensities and their associated uncertainties are given in *relatively calibrated energy units* in column (4) of Table 1. Comprehensive, absolutely calibrated line lists will be published later.

3. RELATIVE RADIOMETRIC CALIBRATION

The efficiency of the SERTS-95 multilayer-coated grating was directly measured at the Synchrotron Ultraviolet Radiation Facility of the National Institute of Standards and Technology (NIST). Unfortunately, the configuration of that facility at the

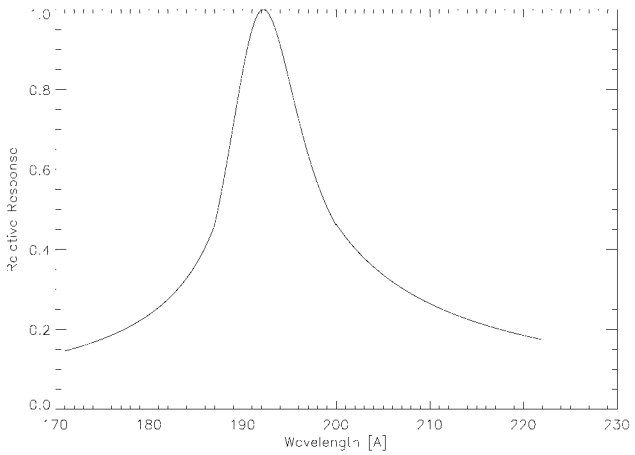

FIG. 1.—The SERTS-95 second-order relative radiometric response normalized to its maximum value around 192 Å, derived from density- and temperature-insensitive line intensity ratios. The curve is narrow and sharply peaked because of the multilayer coating on the toroidal diffraction grating.

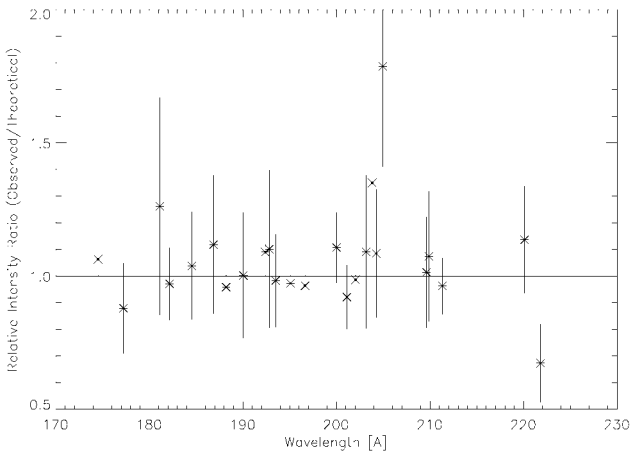

FIG. 2.—Plot of the observed–to–theoretical intensity ratios (col. [6] of Table 1), normalized to the weighted average ratio within each line group, as a function of wavelength. The zero slope indicates that there is no wavelength bias in the derived calibration curve. The mutual consistency of the ratios demonstrates both the validity of the derived calibration and the accuracy of the atomic physics parameters.

time was not well suited for distinguishing first- and second-order effects, and so a reliable, usable calibration curve could not be derived. We therefore used available density- and temperature-insensitive line intensity ratios from the spatially averaged solar active region spectrum itself in order to derive the SERTS-95 second-order relative radiometric calibration. Such an approach was proposed by Neupert & Kastner (1983) as a means of monitoring relative calibration variations of in-flight EUV spectrometers, and it was used by Brosius et al. (1996a) to adjust the laboratory calibration curve for SERTS-91 and SERTS-93.

We used the CHIANTI (version 1.01) package (Dere et al. 1997) to obtain theoretical density- and temperature-insensitive line intensity ratios of emission lines in the SERTS-95 second-order wave band. These include lines from Fe x through Fe XIV. The adopted lines are listed in Table 1, in which the first two columns identify the line by ion and wavelength, and the third column provides the theoretical intensity in energy units normalized to one selected line in each given series. Some of the line intensity ratios exhibit slight variations with density. These are indicated as uncertainties on the normalized theoretical intensities, where the uncertainty corresponds to half of the difference between the maximum and minimum values within the range $8.5 \leq \log n_e \leq 10.5$. In each case, the intensity ratios were calculated at the temperature of maximum ion abundance (i.e., the lines' "formation temperature"), using the Arnaud & Raymond (1992) ionization equilibrium calculations. (Using the Arnaud & Rothenflug 1985 calculations produces no change.)

The SERTS-95 second-order relative radiometric calibration was derived by obtaining factors by which the various integrated line intensities in the spatially averaged, uncalibrated active region spectrum must be multiplied in order to obtain agreement between the observed and the theoretical line intensity ratios. The method was essentially one of bootstrapping our way through the spectrum: we interpolated or extrapolated where necessary but always required the multiplication factor for any given line to yield agreement between the observed and corresponding theoretical line intensity ratios. The derived factors were fitted (as a function of wavelength) with a smooth curve composed of three separate least-squares fit polynomials joined continuously, and normalized to the maximum value of the curve. The derived instrumental relative response curve is shown in Figure 1. The peak response occurs at 192 Å, and the width of the curve at half its maximum amplitude (relative to the minimum of the curve) is 14.7 Å. Both of these are consistent with the design characteristics of the multilayer coating and agree at least qualitatively with the NIST measurements. (The shape of the response curve is dominated by that of the multilayer coating because atmospheric absorption, the reflectivity of the telescope, and the transmission of the aluminum filter all vary smoothly and gradually with wavelength.)

The derived relative response curve was applied to the original uncalibrated spectrum, thus yielding a relatively calibrated spectrum. The resultant observed integrated emission-line intensities *in relatively calibrated energy units* are listed in column (4) of Table 1. To facilitate a comparison between these and the corresponding normalized theoretical intensities, we normalized the observed intensities to the same lines used in column (3) within each line group (col. [5]). A line-by-line comparison demonstrates excellent agreement between similarly normalized theoretical and observed values. This is illustrated in Figure 2, where we plot the ratios and associated 1 σ uncertainties of the relative observed intensities to the relative theoretical intensities (col. [6] of Table 1, normalized by the weighted average ratio within each group) as a function of wavelength. The fact that no slope is evident in this figure indicates that there is no wavelength bias in the derived relative radiometric calibration curve. Furthermore, the fact that so many line intensity ratios from five successive ionization stages of iron yield mutually consistent results confirms the validity of the atomic physics calculations.

Three of the observed lines in Table 1 are actually self-blends of closely spaced line pairs from a given ion. These include the Fe XII line at 186.867 Å, the Fe XII line at 195.117 Å, and the Fe XIII line at 203.820 Å. Contributions from both components of the above blends were incorporated in all theoretical ratios involving those lines.

All of the lines listed in Table 1 can be used to verify, modify, or derive the relative radiometric calibration of the shortest wavelength channel (151–221 Å) of the *SOHO*/CDS Grazing Incidence Spectrometer (GIS). Such a calibration within this

wave band, as well as among the other three GIS wave bands and the two Normal Incidence Spectrometer (NIS) wave bands, is important for accurately measuring properties of the Sun's EUV-emitting plasma. The GIS spectral resolution (instrumental FWHM) is 400–500 mÅ (Harrison et al. 1997); thus, some of the lines that are resolved by SERTS appear blended with the GIS. We therefore indicate, as footnotes to Table 1, lines observed within ± 0.3 Å of the listed wavelength; the intensities and associated uncertainties (in relatively calibrated energy units) are given in parentheses. This enables an assessment of the contributions of possible blends in the GIS spectra.

4. ELECTRON DENSITIES

Several density-sensitive line intensity ratios are available for the same ions used to derive the SERTS-95 relative radiometric calibration. We again used CHIANTI to obtain the dependence of various line intensity ratios on electron density (evaluated at the temperature of maximum line emissivity), and we derived densities from the corresponding measured ratios by cubic spline interpolation on the theoretical curves. Judging from the relative strengths of the lines themselves as well as the relative weaknesses of possible nearby blends, the following ratios are well suited for density diagnostics with GIS spectra: Fe x λ175.265/λ174.526, Fe x λ175.265/λ184.534, Fe XII λ186.867/λ195.117, Fe XIII λ203.820/λ202.042, Fe XIII λ200.017/λ202.042, and Fe XIV λ219.121/λ211.317. The corresponding derived densities are $9.396^{+0.204}_{-0.246}$, $9.406^{+0.223}_{-0.266}$, $10.08^{+0.21}_{-0.23}$, $9.548^{+0.114}_{-0.119}$, $9.437^{+0.102}_{-0.109}$, and $9.382^{+0.087}_{-0.099}$, where the listed errors are due to measurement uncertainties only. Preliminary results of electron density diagnostics using the GIS are presented by Mason et al. (1997).

5. SUMMARY

We developed and applied a technique for deriving the SERTS-95 relative radiometric calibration by means of density- and temperature-insensitive line intensity ratios. Numerous such ratios of iron lines are mutually consistent and yield an instrumental response curve that matches the design characteristics of the multilayer coating. This supports the accuracy of the atomic physics parameters and indicates that the ratios listed in Table 1 may be used to help confirm or derive the relative radiometric calibration of the short-wavelength channel of the CDS/GIS aboard *SOHO*. Because of freedom from blending with nearby strong lines, the following density-sensitive ratios are particularly well suited for analysis with the GIS: Fe x λ175.265/λ174.526, Fe x λ175.265/λ184.534, Fe XII λ186.867/λ195.117, Fe XIII λ203.820/λ202.042, Fe XIII λ200.017/λ202.042, and Fe XIV λ219.121/λ211.317.

J. W. B. acknowledges NASA support through contract NASW-96006. J. M. D. and R. J. T. acknowledge NASA support for the SERTS program by RTOP grants from the Solar Physics Office of NASA's Space Physics Division. We gratefully acknowledge valuable discussions with E. Landi, P. R. Young, and H. E. Mason.

REFERENCES

Arnaud, M., & Raymond, J. 1992, ApJ, 398, 394
Arnaud, M., & Rothenflug, R. 1985, A&AS, 60, 425
Behring, W. E., Cohen, L., Feldman, U., & Doschek, G. A. 1976, ApJ, 203, 521
Brosius, J. W., Davila, J. M., Thomas, R. J., & Monsignori-Fossi, B. C. 1996a, ApJS, 106, 143
Brosius, J. W., Davila, J. M., Thomas, R. J., Monsignori-Fossi, B. C., & Jordan, S. D. 1996b, in UV and X-Ray Spectroscopy of Astrophysical and Laboratory Plasmas, ed. K. Yamashita & T. Watanabe (Tokyo: Universal Academy Press), 83
Brosius, J. W., Davila, J. M., Thomas, R. J., Saba, J. L. R., Hara, H., & Monsignori-Fossi, B. C. 1997a, ApJ, 477, 969
Brosius, J. W., Davila, J. M., Thomas, R. J., & White, S. M. 1997b, ApJ, 488, 488
Brosius, J. W., et al. 1993, ApJ, 411, 410
Davila, J. M., Thomas, R. J., Thompson, W. T., Keski-Kuha, R. A. M., & Neupert, W. M. 1993, in UV and X-Ray Spectroscopy of Astrophysical and Laboratory Plasmas, ed. E. Silver & S. Kahn (Cambridge: Cambridge Univ. Press), 301
Dere, K. P. 1978, ApJ, 221, 1062
Dere, K. P., Landi, E., Mason, H. E., Monsignori-Fossi, B. C., & Young, P. R. 1997, A&AS, 125, 149
Dere, K. P., Mason, H. E., Widing, K. G., & Bhatia, A. K. 1979, ApJS, 40, 341
Harrison, R. A., et al. 1997, Sol. Phys., 170, 123
Landi, E., Del Zanna, G., Landini, M., Bromage, B. J. I., Breeveld, E. R., & Pike, C. D. 1998a, in preparation
Landi, E., Landini, M., Pike, C. D., & Mason, H. E. 1998b, Sol. Phys., in press
Mason, H. E., Young, P. R., Pike, C. D., Harrison, R. A., Fludra, A., Bromage, B. J. I., & Del Zanna, G. 1997, Sol. Phys., 170, 143
Neupert, W. M., Epstein, G. L., Thomas, R. J., & Thompson, W. T. 1992, Sol. Phys., 137, 87
Neupert, W. M., & Kastner, S. O. 1983, A&A, 128, 188
Thomas, R. J., & Neupert, W. M. 1994, ApJS, 91, 461
Thompson, W. T., Neupert, W. M., Jordan, S. D., Jones, H. P., Thomas, R. J., & Schmieder, B. 1993, Sol. Phys., 147, 29
Tousey, R., Bartoe, J.-D. F., Brueckner, G. E., & Purcell, J. D. 1977, Appl. Opt., 16, 870
Young, P. R., Landi, E., & Thomas, R. J. 1998, A&A, 329, 291